differences in ion infrared band strengths with respect to the neutrals[27], only a small excess of ions would be necessary to reproduce the UIRs, so long as these ions consistently exhibit strong features at 6.2 and 11.2 μm, and exhibit a lack of strong features at other non-UIR wavelengths. Hence it appears essential to extend the laboratory experiments described here to ionized PAHs to assess definitively the PAH hypothesis. We note that the general mechanism proposed for production of the UIRs (ultraviolet absorption followed by internal conversion and infrared emission)[4,5] is quite strongly supported by our measurements, as well as by earlier measurements of ultraviolet-laser-excited PAHs[13,16,17,28,29] in the 3-μm region. □

Received 20 June 1995; accepted 6 February 1996.

1. Snow, T. P. & Witt, A. N. *Science* **270,** 1455–1460 (1995).
2. Tielens, A. G. G. M. in *Carbon in the Galaxy: Studies From Earth and Space* (eds Tarter, J. C., Chan, S. & DeFrees, D. J.) 59–111 (NASA Conf. Publ. 3061, Moffett Field, 1987).
3. Cadwell, B. J., Wang, H., Feigelson, E. D. & Frenklach, M. *Astrophys. J.* **429,** 285–299 (1994).
4. Allamandola, L. J., Tielens, A. G. G. M. & Barker, J. R. *Astrophys. J. Suppl. Ser.* **71,** 733–775 (1989).
5. Léger, A. & d'Hendecourt, L. *Ann. Phys. Fr.* **14,** 181–206 (1989).
6. Cohen, M. *et al. Astrophys. J.* **341,** 246–269 (1989).
7. Geballe, T. R., Lacy, J. H., Persson, S. E., McGregor, P. J. & Soifer, B. T. *Astrophys. J.* **292,** 500–505 (1985).
8. Witteborn, F. C. *et al. Astrophys. J.* **341,** 270–277 (1989).
9. de Muizon, M. J., d'Hendecourt, L. B. & Geballe, T. R. *Astr. Astrophys.* **235,** 367–378 (1990).
10. Schutte, W. A., Tielens, A. G. G. M., Allamandola, L. J., Cohen, M. & Wooden, D. H. *Astrophys. J.* **360,** 577–589 (1990).
11. Allamandola, L. J. *et al. Astrophys. J.* **345,** L59–L62 (1989).
12. Petroff, M. D., Stapelbroek, M. G. & Kleinhans, W. A. *Appl. Phys. Lett.* **51,** 406–408 (1987).
13. Schlemmer, S. *et al. Science* **265,** 1686–1689 (1994).
14. Allamandola, L. J., Tielens, A. G. G. M. & Barker, J. R. *Astrophys. J.* **290,** L25–L28 (1985).
15. Léger, A. & Puget, J. L. *Astr. Astrophys.* **137,** L5–L8 (1984).
16. Shan, J., Suto, M. & Lee, L. C. *Astrophys. J.* **383,** 459–465 (1991).
17. Williams, R. M. & Leone, S. R. *Astrophys. J.* **443,** 675–681 (1995).
18. Flickinger, G. C., Wdowiak, T. J. & Gómez, P. L. *Astrophys. J.* **380,** L43–L46 (1991).
19. Joblin, C., d'Hendecourt, L., Léger, A. & Défourneau, D. *Astr. Astrophys.* **281,** 923–936 (1994).
20. Joblin, C., Boissel, P., Léger, A., d'Hendecourt, L. & Défourneau, D. *Astr. Astrophys.* **299,** 835–846 (1995).
21. Allamandola, L. J., Sandford, S. A., Hudgins, D. M. & Witteborn, F. C. in *Airborne Astronomy Symposium on the Galactic Ecosystem* (eds Haas, M. R., Davidson, J. A. & Erickson, E. F.) 23–32 (Astronomical Soc. of the Pacific, San Francisco, 1995).
22. Hudgins, D. M. & Allamandola, L. J. *J. phys. Chem.* **99,** 3033–3046 (1995).
23. Szczepanski, J. & Vala, M. *Astrophys. J.* **414,** 646–655 (1993).
24. Szczepanski, J., Chapo, C. & Vala, M. *Chem. Phys. Lett.* **205,** 434–439 (1993).
25. Vala, M. *et al. J. phys. Chem.* **98,** 9187–9196 (1994).
26. Omont, A. *Astr. Astrophys.* **164,** 159–178 (1986).
27. Langhoff, S. R. *J. phys. Chem.* (in the press).
28. Brenner, J. & Barker, J. R. *Astrophys. J.* **388,** L39–L43 (1992).
29. Cherchneff, I. & Barker, J. R. *Astrophys. J.* **341,** L21–L24 (1989).

ACKNOWLEDGEMENTS. This work was supported by the NASA Astrophysics Program, the NASA Exobiology Program, and fellowships from the Deutsche Forschungsgemeinschaft (S.S.), the Consiglio Nazionale delle Recerche (Italy) (N.B.) and the Max-Plank-Gesellschaft and the Alexander von Humboldt Stiftung (B.S.).

Discovery of an extended sodium atmosphere around Europa

Michael E. Brown* & Richard E. Hill

Lunar and Planetary Laboratory, University of Arizona, Tucson, Arizona 85721, USA

Europa, one of the satellites of Jupiter, has long been thought to be a dormant icy body[1], unlike its volcanically active neighbour, Io. Europa lies deep within Jupiter's magnetosphere, however, and is continuously bombarded by energetic ions, which modify the surface ices[2] and are probably responsible for creating Europa's tightly bound oxygen atmosphere[3,4]. Here we report the discovery of an atmosphere of atomic sodium that extends to at least 25 times Europa's radius. We suggest that this sodium is originally released by Io's volcanoes, after which it is ionized in the magnetosphere and implanted into Europa's surface ice; subsequent sputtering of the ice by magnetospheric ions releases the sodium to form the extended atmosphere. Although sodium is a minor constituent of Europa's atmosphere, it traces the distribution of the major atmospheric components which are not themselves directly observable. The sodium and oxygen could represent the extremes of the distribution of the atmospheric components, with only the heaviest molecules (such as the oxygen) being tightly bound; alternatively the sodium might be in the form of an extended corona, analogous to Io's atmosphere.

Observations of sodium around Europa were made on 5 June 1995 using an echelle spectrograph[5] on the 1.53-m University of Arizona telescope on Mt Bigelow. We obtained ten long-slit high-resolution (0.25 Å) spectra of Europa, each with the slit oriented perpendicular to Europa's orbital plane, and covering the wavelengths between 5,883 and 5,904 Å, which includes the sodium D_1 and D_2 lines at 5,895.92 and 5,889.95 Å, respectively. Table 1 gives a log of the observations. All spectra were obtained when Europa was far from Io to minimize contamination from sodium emitted from Io, but faint Io sodium is still likely to be present as a spectrally and spatially diffuse background. Observations of the disk of Jupiter were obtained for intensity calibration. (We assume 5.5 MR $Å^{-1}$ for the peak intensity of the disk[6], where $1\,R = (1/4\pi) \times 10^6$ photons $cm^{-2}\,s^{-1}\,sr^{-1}$.) Because terrestrial sodium emission (intensity ~100 R) is uniform across the spatial dimension of the slit and is Doppler-shifted from Europa sodium by −0.15 Å (−7 km s^{-1}), it is readily subtracted. The same subtraction removes the uniformly distributed Io sodium. Figure 1 shows a typical spectrum of Europa and of the sodium emission. The observed emission lines are centred at wavelengths of 5,895.77 and 5,889.80 Å, precisely those expected for sodium at Europa's velocity, and the emission is strongly peaked at the spatial position of Europa. We therefore conclude that Europa is the source of the sodium. No changes are observable during the

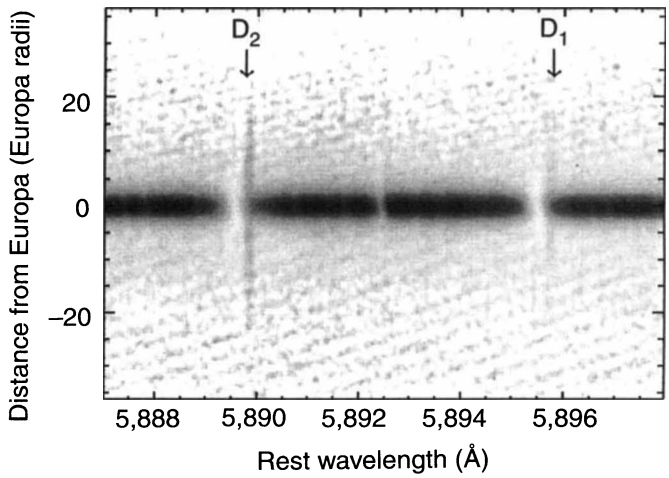

FIG. 1 A long-slit high-resolution spectrum of Europa showing sodium emission. The dark horizontal band is a spectrum of reflected sunlight from Europa's surface in which solar Fraunhofer absorption features are visible (including the strong sodium absorptions). The sodium emission lines are marked by D_2 and D_1 and can be traced to at least 25 Europa radii. The spectral slit was oriented perpendicular to the orbital plane, so the sodium emission seen is from north and south of the satellite. This spectrum has been heavily processed to show the faint sodium emission against the much brighter Europa continuum, and a constant contribution from atmospheric sodium emission has been subtracted.

* Present address: Division of Geological and Planetary Sciences, Mail Stop 170-25, California Institute of Technology, Pasadena, California 91125, USA.

4.5 hours of observations, so we add together all spectra to increase the signal-to-noise ratio.

The observed spatial distribution of sodium emission around Europa is shown in Fig. 2. Because of the overwhelming brightness of the Europa continuum, the emission intensity inside $\sim 5 R_e$ (where R_e is a distance equal to Europa's 1,569-km radius) cannot be quantified. The ratio of the intensities of the D_2 and D_1 lines is 1.70 ± 0.05, consistent with the expected value of 1.66 for optically thin emission and resonant scattering of sunlight[6]; therefore the line-of-sight column density of sodium (shown on the right-hand vertical axis of Fig. 2) is directly proportional to the emission intensity. Figure 3 shows the sodium column density on a log–log scale to illustrate better the atmospheric structure. The best-fit line through these points has a slope of -1.5 ± 0.1. If the sodium is distributed symmetrically around Europa, this slope implies a total mass of sodium between 1 and 25 R_e of ~840 kg and a density at Europa's surface of ~70 atoms cm^{-3}. This sodium surface density is 100 times smaller than the extrapolated surface density of sodium at Io[7].

TABLE 1 Observations of Europa spectra

Start time (UT)	Exposure time (min)	Air mass	Europa phase (deg)	Io phase (deg)
04:11	20	2.60	91	227
04:34	20	2.21	93	230
05:24	20	1.91	96	237
05:47	30	1.81	98	240
06:18	30	1.72	100	245
06:58	30	1.68	103	251
07:30	30	1.70	105	255
08:09	30	1.78	108	261
08:42	30	1.90	110	265
09:21	20	2.18	113	271

The extent of the sodium distribution implies that atoms are leaving the surface at high velocity: to reach a height of 25 R_e above a pole of Europa requires a velocity greater than 2 km s^{-1}. Preliminary modelling of particle trajectories suggests that most of the particle velocities must be this large or larger to avoid the accumulation of gravitationally bound particles close to Europa and account for the flatness of the profile between 5 and 10 R_e. As sublimation at the Europa surface temperature of 95 K will produce typical velocities of only 0.3 km s^{-1}, the most likely mechanism for generating the required high velocities is sputtering by energetic magnetospheric particles[4].

Sodium must be present on Europa's surface in order to be sputtered into the atmosphere. A potential sodium source is ions transported outward from Io and implanted into the surface ice of Europa. Knowing the ion implantation rate and the lifetime for atmospheric sodium, we can calculate the total mass due to this source and compare it to the observed sodium mass. At Europa, the magnetospheric ion density is ~80 ions cm^{-3} (ref. 8), of which ~1% is thought to be sodium[7], and the ions sweep past at ~100 km s^{-1} (ref. 9), producing an implantation rate into Europa's surface of 24 g s^{-1} of sodium. All of this sodium is subsequently removed by sputtering: implantation depths are at most ~100 Å, so the sodium is removed within at most 100 yr (ref. 4). Once removed from the surface, neutral sodium will be destroyed by electron impact ionization or transported beyond the 25-R_e radius that we have observed. The lifetime of neutral sodium against electron impact ionization is between 20 and 100 h, depending on the local magnetospheric electron density[8,10]. The transport time for particles with initial velocities between 2 and 2.4 km s^{-1} to escape past 25 R_e is 10–30 h. Assuming a mean combined lifetime of 20 h due to both processes, the steady-state mass of sodium surrounding Europa from this source should be ~1,700 kg, within a factor of two of the observed amount.

Naturally occurring sodium impurities in Europa's surface ice might also contribute to the atmosphere. Assuming the cosmic Na : O ratio of 1 : 370 (ref. 11) and using Johnson's estimate for the water sputtering rate[4] of 10^8–10^{10} molecules cm^{-2} s^{-1}, the sodium removal rate is 1–100 g s^{-1}. At the upper limit of the range, this source exceeds the implantation source, but the sputtering rate and intrinsic sodium abundance are both highly uncertain. Because of this uncertainty and because the implantation source must be present at approximately the levels calculated, we conclude that implantation and sputtering of Io sodium is probably the dominant source of the Europa sodium. If true, this sodium atmosphere is the first known example of an atmospheric constituent captured from an external moon or planet.

Although sodium is only a minor species, with a total mass 300

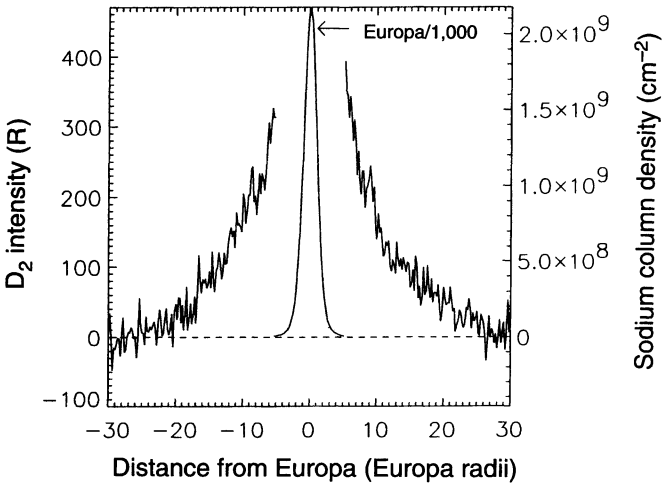

FIG. 2 A profile of the D_2 sodium emission intensity and of the sodium column density. The smooth curve labelled 'Europa/1,000' shows the emission intensity of Europa, divided by 1,000, and demonstrates the spatial resolution of the data. Inside 5 Europa radii, the sodium emission intensity cannot be determined because it is overwhelmed by the much brighter Europa continuum.

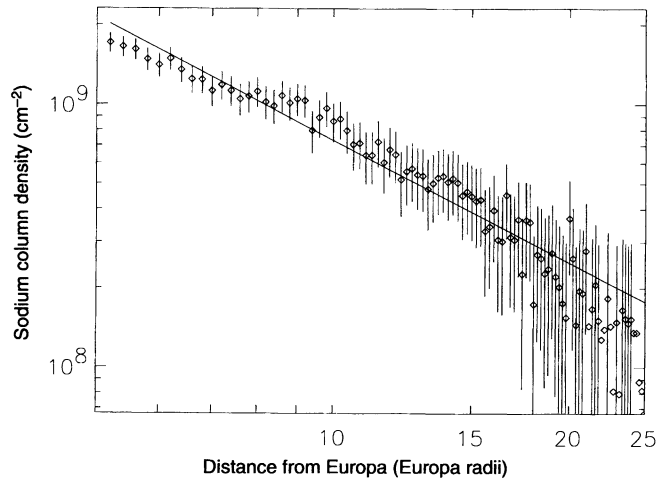

FIG. 3 A log–log plot of the sodium column density. The best-fit-line through these data has a slope of −1.5. Assuming spherical symmetry, the total mass implied by this slope is 840 kg.

times less than that of the closely confined O_2 atmosphere, the sodium traces the behaviour of the dominant sputtered water products that are not directly observable. These observations therefore show that the Europa atmosphere contains a significant escaping component in addition to the bound component previously observed. These two components could represent the extremes of a single energy distribution, with the more massive O_2 having low velocity and remaining bound, and the lighter sodium atoms (and even lighter water products) acquiring high velocity and escaping. In this case, the atmosphere would be predominantly escaping with only the heavy O_2 tightly bound. Alternatively, Europa's atmosphere may be more analogous to Io's, with a bound collisionally thick lower atmosphere and an extended corona sputtered from this bound component. In this case, the bound atmosphere would contain significant amounts of water products and of sodium, in addition to the observed O_2, and the sputtered corona would contain a representative sample of this atmosphere. Further understanding of the structure and nature of Europa's atmosphere will require observations to link the bound and escaping components, detecting either oxygen further out or sodium closer in to the satellite. The accessibility of sodium emissions to ground-based telescopes suggests that sodium observations will be most useful for advancing our understanding of this satellite and its atmosphere. □

Received 28 July 1995; accepted 29 January 1996.

1. Clark, R. N., Fanale, F. P. & Gaffey, M. J. in *Satellites* (eds Burns, J. A. & Matthews, M. S.) 437–491 (Univ. Arizona Press, Tucson, 1986).
2. Johnson, R. E., Nelson, M. L., McCord, T. B. & Gradie, J. C. *Icarus* **75,** 423–436 (1988).
3. Hall, D. T., Strobel, D. F., Feldman, P. D., McGrath, M. A. & Weaver, H. A. *Nature* **373,** 677–679 (1995).
4. Johnson, R. E. *Energetic Charged-Particle Interactions with Atmospheres and Surfaces* (Springer, Berlin, 1990).
5. Hunten, D. M., Wells, W. K., Brown, R. A., Schneider, N. M. & Hilliard, R. L. *Publs astr. Soc. Pacif.* **103,** 1187–1192 (1991).
6. Brown, R. A. & Yung, Y. L. in *Jupiter* (ed. Gehrels, T.) 1102–1145 (Univ. Arizona Press, Tucson, 1976).
7. Schneider, N. M., Hunten, D. M., Wells, W. K., Schultz, A. B. & Fink, U. *Astrophys. J.* **368,** 298–314 (1991).
8. Bagenal, F. *J. geophys. Res.* **99,** 11043–11062 (1994).
9. McNutt, R. L., Belcher, J. W., Sullivan, J. D., Bagenal, F. & Bridge, H. S. *Nature* **280,** 803–804 (1979).
10. Smyth, W. H. & Combi, M. *Astrophys. J.* **328,** 888–918 (1988).
11. Allen, C. W. *Astrophysical Quantities* (Athlone, London, 1973).

ACKNOWLEDGEMENTS. We thank E. J. Moyer, A. J. Dessler and D. M. Hunten for enlightening conversations. This work was supported by a Hubble Fellowship grant from STScI.

Yttrium and lanthanum hydride films with switchable optical properties

J. N. Huiberts, R. Griessen, J. H. Rector, R. J. Wijngaarden, J. P. Dekker, D. G. de Groot & N. J. Koeman

Faculty of Physics and Astronomy, Vrije universiteit, De Boelelaan 1081, 1081 HV Amsterdam, The Netherlands

In many substances, changes in chemical composition, pressure or temperature can induce metal-to-insulator transitions[1]. Although dramatic changes in optical and electrical properties accompany such transitions, their interpretation is often complicated by attendant changes in crystallographic structure[2]. Yttrium, lanthanum and the trivalent rare-earth elements form hydrides that also exhibit metal–insulator transitions[3–5], but the extreme reactivity and fragility of these materials hinder experimental studies[5,6]. To overcome these difficulties, we have coated thin films of yttrium and lanthanum with a layer of palladium through which hydrogen can diffuse. Real-time transitions from metallic (YH_2 or LaH_2) to semiconducting (YH_3 or LaH_3) behaviour occur in these films during continuous absorption of hydrogen, accompanied by pronounced changes in their optical properties. Although the timescale on which this transition occurs is at present rather slow (a few seconds), there appears to be considerable scope for improvement through the choice of rare-earth element and by adopting electrochemical means for driving the transition. In view of the spectacular changes in optical properties—yttrium hydride, for example, changes from a shiny mirror to a yellow, transparent window—metal hydrides might find important technological applications.

In some cases metal–insulator transitions can be induced by varying continuously an externally controlled parameter such as pressure or temperature. A well known example is that of VO_2 which exhibits a semiconductor-to-metal transition around 340 K during heating[2]. At the transition the electrical conductivity changes abruptly although the optical properties at visible wavelengths are only weakly modified. From a fundamental point of view, the interpretation of the metal–insulator transition in VO_x is complicated by the drastic crystallographic changes (distorted monoclinic to tetragonal) which occur at the transition. Another class of solids exhibiting a metal–insulator transition is that of the trihydride-forming metals, Y, La and the trivalent rare-earths (RE)[3–5].

Unfortunately bulk samples of YH_x, LaH_x and REH_x often fall apart into powder when x approaches 3 (refs 5,6), severely limiting the possibility of investigating their electrical and optical properties. The nature of the electronic ground state of the trihydrides has accordingly not been firmly established[7]. By evaporating films one might improve the structural stability of the trihydrides. However, thin films of Y, La and RE are extremely reactive and thus difficult to handle. To circumvent these difficulties, we evaporated yttrium films under ultra-high vacuum (UHV; 10^{-6} Pa during evaporation) conditions and coated them with a thin layer of palladium (5–20 nm thick) through which hydrogen may pass to, or from, the (typically 500-nm-thick) yttrium film. The palladium overlayer protects the yttrium film from oxidation so effectively that the samples could be transferred without special precautions to *ex situ* experimental setups. These samples made possible a comprehensive study of properties of YH_x ($0 \leqslant x < 3$), such as electrical resistivity ρ, magnetoresistance, photoconductivity, Hall effect and optical transmission as a function of temperature (between 4.2 and 300 K), magnetic field (between 0 and 7 T) and composition (J.N.H. *et al.*, manuscript in preparation). As far as a comparison with bulk YH_x is possible (for electrical resistivity data, x is limited to < 2.1) our YH_x films exhibit the characteristic features of bulk YH_x samples. For example, the temperature dependence of ρ exhibits the 175 K anomaly in the α^*-YH_x phase[8] and the hydrogen-concentration dependence of ρ shows a pronounced minimum in the β-YH_2 phase and a rapid increase in the γ-YH_3 phase. The lattice spacings of the film (a) are also very close to the bulk values (for example, $a = 5.219$ Å (YH_2-film), $a = 5.205$ Å (ref. 9), 5.201 Å (ref. 10), 5.209 Å (ref. 11) (bulk YH_2)). Thermodynamically, YH_x films are slightly less stable than bulk YH_x, the enthalpy of formation for our films $\Delta H_{\beta\rightarrow\gamma} \approx -38$ kJ per mol H being 6 kJ per mole H higher than that of bulk samples[12]. This well known effect is due to the fact that the effective attractive H–H interaction in metal hydrides is essentially of elastic origin[13]. The partial clamping of the film by the substrate leads to a weakening of the H–H interaction and consequently to an increase in $\Delta H_{\beta\rightarrow\gamma}$. For the present study, this is an advantage because it allows the removal of hydrogen from YH_3 to give YH_2 without having to use UHV pumping. With our thin-film technique we have also recently succeeded in producing stoichiometric YH_3 by loading Y under very high pressures (up to 25 GPa of hydrogen) in a diamond anvil cell. The changes in properties of YH_x as a function of x obtained by simply subjecting a 500-nm–thick film of Y (with a 20-nm Pd cap layer) to 10^5 Pa of hydrogen gas are, however, very interesting, and we describe them here.